Hindawi
International Journal of Photoenergy
Volume 2018, Article ID 7506151, 12 pages
https://doi.org/10.1155/2018/7506151

Research Article

C-, N-, S-, and F-Doped Anatase TiO_2 (101) with Oxygen Vacancies: Photocatalysts Active in the Visible Region

Julio César González-Torres,[1] Enrique Poulain,[1] Víctor Domínguez-Soria,[2] Raúl García-Cruz,[1] and Oscar Olvera-Neria[1]

[1]*Área de Física Atómica Molecular Aplicada (FAMA), CBI, Universidad Autónoma Metropolitana-Azcapotzalco, Av. San Pablo 180, Col. Reynosa Tamaulipas, 02200 Ciudad de México, Mexico*
[2]*Área de Química Aplicada, CBI, Universidad Autónoma Metropolitana-Azcapotzalco, Av. San Pablo 180, Col. Reynosa Tamaulipas, 02200 Ciudad de México, Mexico*

Correspondence should be addressed to Oscar Olvera-Neria; oon@correo.azc.uam.mx

Received 22 February 2018; Accepted 6 May 2018; Published 10 June 2018

Academic Editor: Xuxu Wang

Anatase TiO_2 presents a large bandgap of 3.2 eV, which inhibits the use of visible light radiation ($\lambda > 387$ nm) for generating charge carriers. We studied the activation of TiO_2 (101) anatase with visible light by doping with C, N, S, and F atoms. For this purpose, density functional theory and the Hubbard U approach are used. We identify two ways for activating the TiO_2 with visible light. The first mechanism is broadening the valence or conduction band; for example, in the S-doped TiO_2 (101) system, the valence band is broadened. A similar process can occur in the conduction band when the undercoordinated Ti atoms are exposed on the TiO_2 (101) surface. The second mechanism, and more efficient for activating the anatase, is to generate localized states in the gap: N-doping creates localized empty states in the bandgap. For C-doping, the surface TiO_2 (101) presents a "cleaner" gap than the bulk TiO_2, resulting in fewer recombination centers. The dopant valence electrons determine the number and position of the localized states in the bandgap. The formation of charge carriers with visible light is highly favored by the oxygen vacancies on TiO_2 (101). The catalytic activity of C-doping using visible radiation can be explained by its high absorption intensity generated by oxygen vacancies on the surface. The intensity of the visible absorption spectrum of doped TiO_2 (101) follows the order: C > N > F > S dopant.

1. Introduction

In the late '70s, photocatalysis took a turn when researchers discovered the TiO_2 ability to degrade stable organic compounds as they were studying the water photoelectrolysis [1–3]. Since then, there has been a great interest to improve the degradation efficiency of organic pollutants using TiO_2 [4–7].

Anatase TiO_2 has an energy bandgap of 3.2 eV, that is, UV radiation is mandatory to promote electrons from the valence band (VB) to the conduction band (CB). Until now, the primary challenge has been to generate charge carriers using visible light rather than UV radiation. Different methodologies have been used to modify the TiO_2 absorption properties, such as doping with transition metals [8–14] or main group elements [15–24], and synthesize composites like ZrO_2/TiO_2, reducing the recombination of charge carriers by aligning the energy gaps [25, 26]. Charge carriers act as oxidation and reduction centers, which enable the creation of reactive species such as hydroxyl radicals, peroxides, or acid compounds. These species promote the degradation of pollutants [27–29].

Atanelov et al. [15] theoretically studied TiO_2 doped with C and N atoms at two different concentrations. They found that dopants decrease the bandgap, which enhances the TiO_2 photocatalytic activity. It is crucial that states created by doping process localize close to the valence band maximum (VBM) or the conduction band minimum (CBM), since states spread along the bandgap may act as a recombination center [15, 30–32]. Sakthivel and Kisch [33] found that

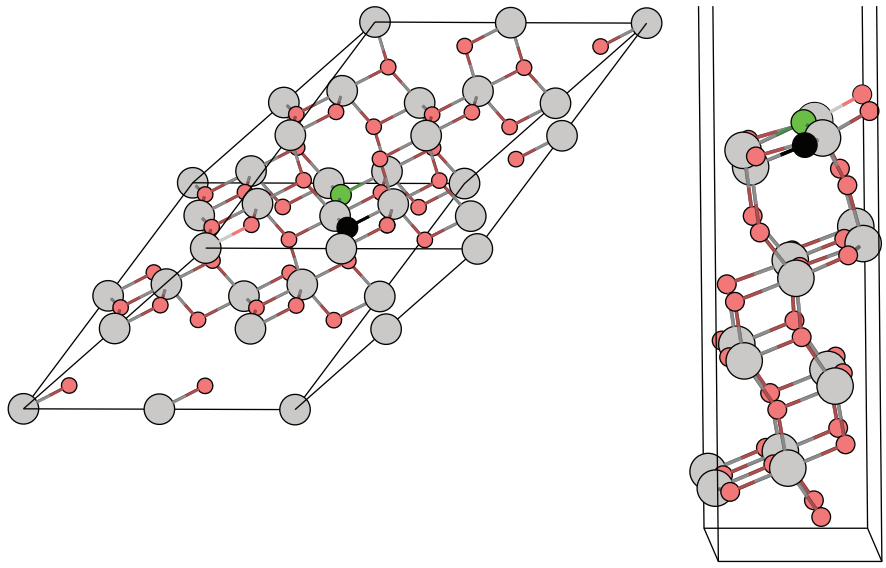

(a) (b)

Figure 1: Doping sites on anatase TiO_2. (a) The $3 \times 3 \times 3$ bulk supercell. (b) The $2 \times 1 \times 1$ surface in the (101) direction with four layers. Both models constituted by 48 atoms. One three-coordinated O atom was replaced by C, N, S, or F atom. Red balls are O atoms; gray ones are Ti. Black balls indicate the substitution site, and green balls show the oxygen vacancy.

C-doping TiO_2 is five times more efficient than N-doping in the degradation of 4-chlorophenol when artificial light ($\lambda \geq 455$ nm) is used. Tian and Liu [34] showed that high S concentrations as a TiO_2 dopant induced a light absorption redshift. Whereas F-doped TiO_2 does not reduce the bandgap [16, 35], Yu et al. [36] obtained a gap of 2.90 eV for an anatase and rutile mixture doped with F^- ions, where the interface may reduce the recombination of photogenerated electrons and holes. Czoska et al. [16] reported that Ti^{3+} states separate from the CBM when the local density approximation (LDA) + U parameter method is used, making this procedure suitable to describe the F-doping on the anatase TiO_2.

TiO_2 usually presents oxygen vacancies; these defects can be controlled experimentally based on nonstoichiometric conditions of synthesis (Ti excess or oxygen deficiency) or by heating the sample in a vacuum at 900 K [37–39]. Zhang et al. [40] showed that there is a synergistic effect of N dopant and oxygen vacancy in TiO_2 contributing to the significant enhancement of the visible light photoactivity. The synergy between species N-Ti and the oxygen vacancy also occurs in heterojunctions such as NiO/N-TiO_2 catalysts [41], but in general, doped TiO_2 and oxygen vacancies have been studied separately. For other dopants, it is not understood how the simultaneous interaction between dopants and vacancies affects the optical response of the TiO_2 (101) surface in the visible region. This knowledge will help optimize doped TiO_2 for the degradation of organic compounds.

This work aims to make a systematic study on C-, N-, S-, and F-doped TiO_2 (101) to obtain the most suitable element to reduce the bandgap or to generate localized states in the gap. Furthermore, the generalized gradient approximation (GGA) and the Hubbard U method are used to explain the intraband states' nature. Notably, this article focuses on the simultaneous interaction of oxygen vacancies and main group dopants to analyze and evaluate the anatase surface response to the visible radiation.

2. Computational Details

The electronic structure of the anatase TiO_2 (101) surface and bulk doped with the C, N, S, and F elements was studied using the VASP5.4.1 program [42, 43] that implements the density functional theory (DFT) [44, 45]. The Perdew-Burke-Ernzerhof (PBE) functional [46, 47] was used to take into account the exchange-correlation energy within the GGA framework [48–51].

Standard DFT calculations underestimate the bandgap because of its difficulty in representing empty states [52]. For recovering of the electron correlation effects—at least in pairs—and the Ti 3d orbitals additional repulsion, we use the Hubbard U parameter [53] as suggested by Morgade and Cabeza for TiO_2 [54]. A value of $U = 5.5$ eV was considered only for Ti 3d electrons following the recommendation by Calzado et al. [55].

The projector augmented wave (PAW) approach is used for describing the ion-electron interactions [56, 57]. The plane-wave basis for all elements with an energy cutoff of 400 eV was employed throughout calculations. We used a k-point mesh of $3 \times 3 \times 3$ for the bulk systems and $5 \times 5 \times 1$ for the surface. The total energy convergence criterion was 1×10^{-4} eV.

A $3 \times 3 \times 3$ supercell was built for modeling the bulk. The (101) plane is the most stable for anatase TiO_2 [58, 59]. Then, the surface was represented by a $2 \times 1 \times 1$ supercell considering four layers in the (101) direction; both the bulk and surface models contain 48 atoms (see Figure 1). A vacuum

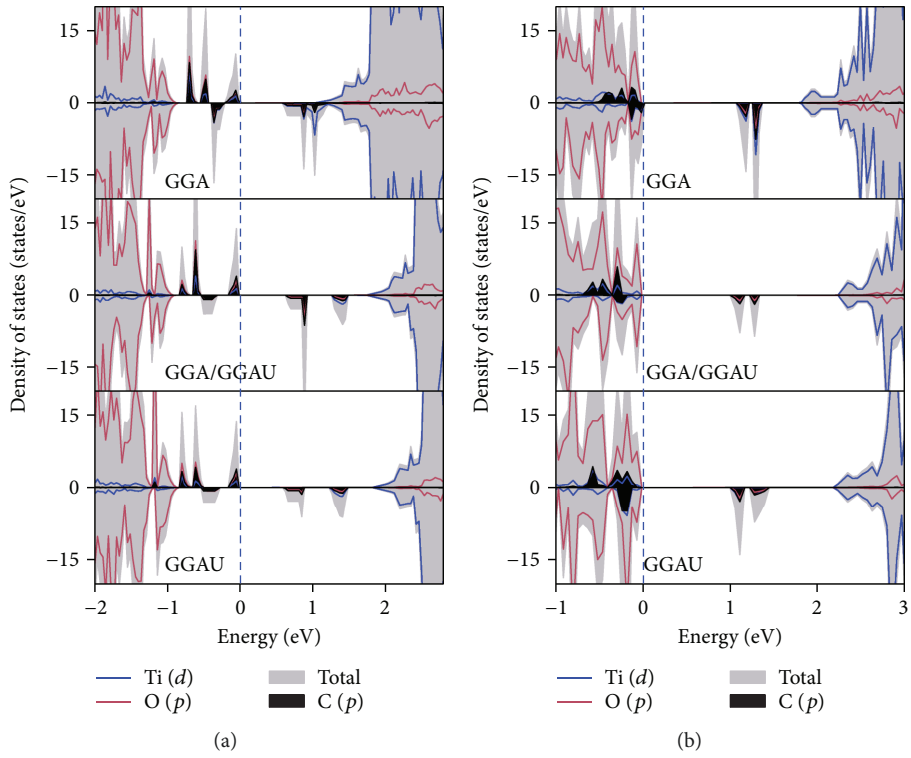

FIGURE 2: The total and partial density of states of the three relaxation methodologies for C-doped anatase TiO_2. (a) The bulk supercell. (b) The TiO_2 (101) surface. The Fermi level corresponds to the zero energy.

of 16 Å was included to ensure that the two adjacent surfaces do not interact.

For the bulk and surface models, the three-coordinated oxygen atom was substituted, yielding a doping concentration of 2.08% mole. On the surface, the second most exposed oxygen atom was replaced by the dopants (see Figure 1(b)). The bottom layer of the slab was constrained to simulate the bulk environment.

Three methodologies were used to study the electronic structure of doped TiO_2. The first, an electronic and geometry relaxation using the PBE functional were performed (GGA); for the second approach, the relaxed geometry obtained by the first method was used to accomplish a single point calculation with the U parameter (GGA/GGAU). Finally, both geometry and electronic relaxation were determined with the U parameter (GGAU). For all calculations, spin polarization was considered.

For studying the simultaneous interaction between impurities and oxygen vacancies, we detach the nearest surface oxygen atom to the dopant on the doped TiO_2 (101); in the pristine TiO_2 surface, we removed the same oxygen for comparison (see Figure 1(b)). The absorption spectra were obtained with the VASPKIT program [60], using the real and imaginary parts of frequency-dependent complex dielectric function [61], after the electronic ground state has been determined. The systems with oxygen vacancies were studied with the GGAU methodology, which represents the most reliable method of those tested in this work.

3. Results and Discussion

The optimized parameters for the bulk TiO_2 are $a = 3.8248$ Å, $c = 9.6909$ Å, and $z = 0.2068$, which agree with experimental values obtained by Horn et al. [62]. For the GGA methodology in the bulk anatase, we obtain an energy bandgap (E_g) of 2.19 eV. For the GGA/GGAU and GGAU methodologies, the E_g broadens to 2.81 and 2.76 eV, respectively, and there are no significant changes in the electronic structure for the bulk system (see Figure S1(a) in the Supplementary Materials). The main effect of the U parameter is to move the Ti $3d$ states toward more positive energies, which increases the bandgap because the CBM is displaced. From now on, every time the three bandgaps are mentioned, we are referring to the values obtained with the GGA, GGA/GGAU, and GGAU approaches.

For the TiO_2 (101) surface, the E_g narrows to 1.85, 2.31, and 2.25 eV for each used methodology, respectively. We attribute this narrowness to the bond unsaturation at the material surface, corresponding to undercoordinated Ti species located at the beginning of the CB, which promotes a bandgap reduction. The density of states (DOS) for the surface depicts characteristic localized empty states below the CB, Figure S1(b). These states have a well-defined shape and are distinct from the occupied states created by the Ti^{3+} species.

3.1. C-Doped TiO_2. For the bulk anatase, C introduces occupied states above the original VB, so the Fermi level is located

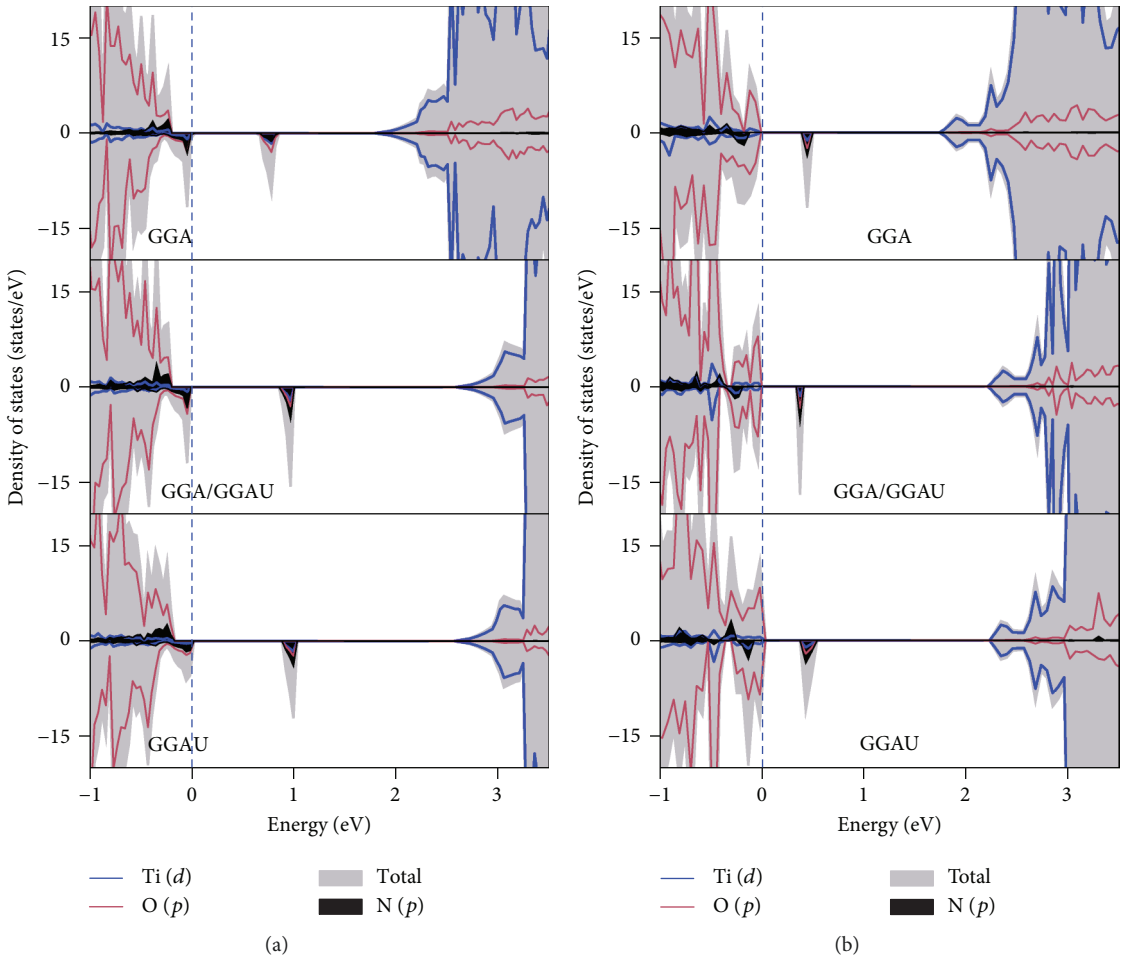

Figure 3: The total and partial density of states of the three relaxation methodologies for N-doped anatase TiO_2. (a) The bulk supercell. (b) The TiO_2 (101) surface.

at the end of these states. Furthermore, C-doping generates unoccupied states that lie in the bandgap region. The calculated bandgaps are 2.44, 2.66, and 2.66 eV (without considering the states introduced by dopants) for the three methodologies (see Figure 2(a) and S2(a)).

The O atoms in the anatase TiO_2 have an oxidation state of −2, which implies that O accepts two electrons in its 2*p* empty orbitals. Carbon has 2 electrons less than O, so its 2*p* orbitals are not going to be full by receiving 2 electrons like O atoms. This process will leave two unoccupied C 2*p* orbitals that are not in the same energy level that Ti 3*d* states therefore will appear below the CB.

When the *U* correlation is considered, the empty states introduced by C-doping are separated from the Ti 3*d* orbitals, and the extra repulsion pushes Ti 3*d* orbitals towards the CBM. This behavior also occurs on the TiO_2 (101) surface; the calculated bandgaps are 1.87, 2.36, and 2.30 eV, which are similar to the pristine system, but the C atom generates two empty states in the bandgap (see Figure 2(b) and S2(b)).

C-doped TiO_2 (101) presents a magnetic moment of 2 μ_B per supercell, which has also been reported for both rutile and anatase phases [15, 63]. Our calculations confirm that one substitutional doping yields a paramagnetic material with a magnetic moment of 2 μ_B, but only 0.70 μ_B on the C atom was measured within the Wigner-Seitz radius of 1.0 Å. The experimental value observed by Ye et al. [64] was 0.0236 μ_B per carbon in carbide state, that is, about 30 times less than the theoretical value.

3.2. N-Doped TiO_2. The N atom has one electron less than O, meaning that charge transfer by Ti will not fulfill all the N 2*p* orbitals, leaving one unpaired electron and also an empty spin-orbital. This process generates N 2*p* localized occupied states at the top of the VB and one empty state in the gap, near the VB (see Figure 3 and S3).

The empty states within the bandgap are not affected by the *U* correlation, which means that they are not hybridized with Ti 3*d* empty orbitals, neither the bulk nor the surface. These results agree with the data reported by Lin et al. [65] for anatase and Atanelov et al. [15] for rutile phase. For N-doped TiO_2, it is easier to excite electrons from the surface (~0.4 eV) than from the bulk system (~1.0 eV), which are in agreement with previous results [66].

On the surface, there is a reduction of the energy bandgap to 2.30 eV (GGAU), whereas the reported experimental value is 2.5 eV [67]. The substitution of O by N leaves an unpaired

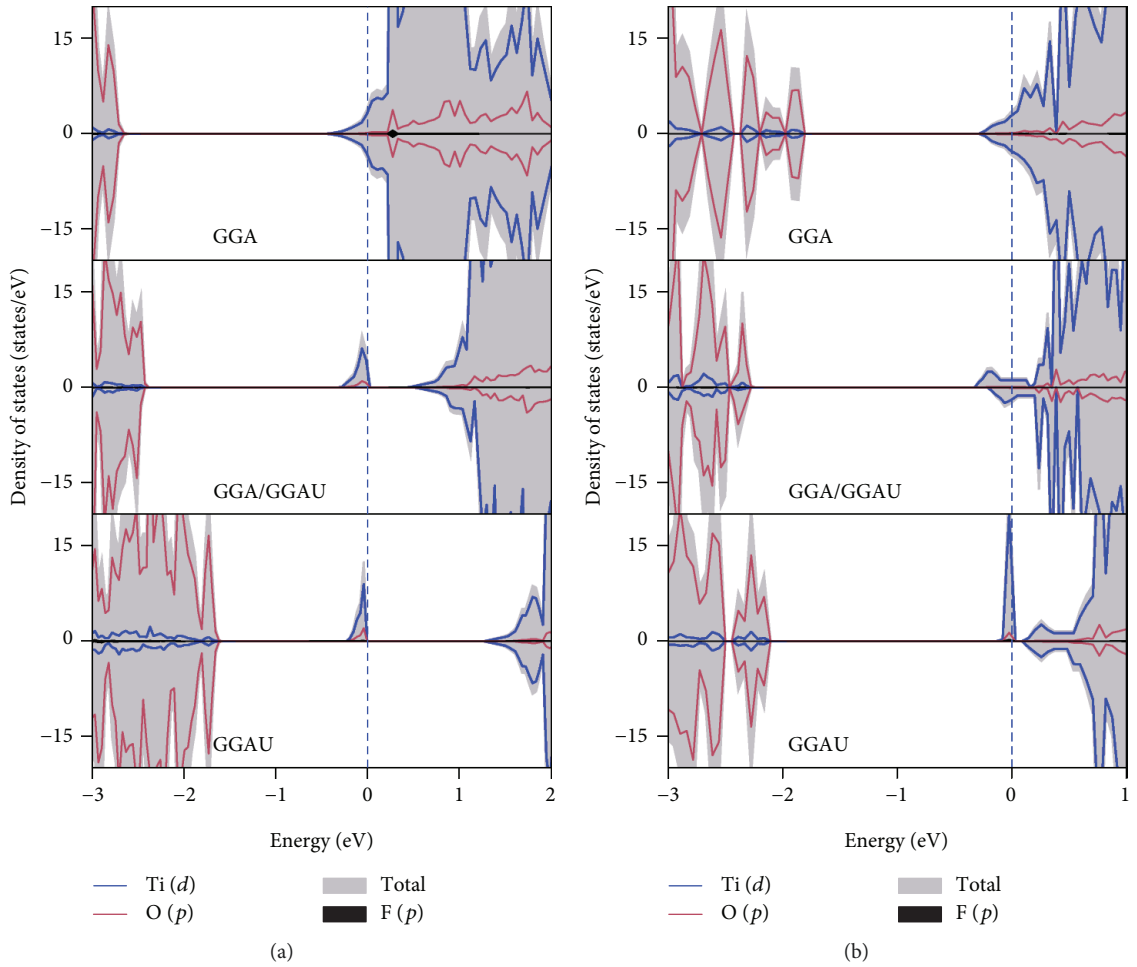

Figure 4: The total and partial density of states of the three relaxation methodologies for F-doped anatase TiO_2. (a) The bulk supercell. (b) The TiO_2 (101) surface.

electron into the system, yielding a magnetic moment of 1 μ_B per supercell, but only 0.503 μ_B on the N atom was measured within the Wigner-Seitz radius of 0.979 Å. An experiment for rutile crystals reported a paramagnetic behavior for the N-doping [68]; our calculations also reproduced this result for the N-doped anatase surface and bulk.

The required energy to obtain charge carries is reduced regarding the pristine TiO_2 due to localized states within the bandgap generated by dopants. C- and N-doped TiO_2 have localized states within the bandgap, reducing the excitation energy, but it has been reported that there is not a direct correlation between the excitation energy to form charge carriers and the photocatalytic activity [69]. The performance of the catalyst also depends on the recombination time, that is, the lifetime before holes and electrons are destroyed by mutual interaction. The position of the localized states within the bandgap affects the recombination time [32].

3.3. F-Doped TiO_2. The F atom has one electron more than oxygen. The substitution of F^- instead of O^{2-} in the lattice leaves one unpaired electron; F can accept only one electron to acquire its closed shell configuration [36]. There are three possible configurations for F-doped TiO_2: (i) the unpaired electron locates in the surrounds of the fluorine; (ii) fluorine transfers the one electron excess to their neighbors, or (iii) the unpaired electron delocalizes within the CB. As Di Valentin et al. [70] have pointed out, the last two options have the same probability of occurrence.

Our results show that the Fermi level is displaced towards the CB, and for the bulk and surface, the GGA method delocalizes the electron in the conduction band. For the bulk system, adding the U correlation parameter to the bulk system localizes occupied states below the CB, separated by 0.6 and 1.31 eV for the GGA/GGAU and GGAU methods (see Figure 4(a) and S4(a)). These occupied states are Ti 3*d* orbitals, so it confirms the charge transfer and the reduction from Ti^{4+} to Ti^{3+}. The surface system, with the GGA/GGAU scheme, does not bring a clear picture of these Ti^{3+} states; it seems these states are degenerated with the Ti surface states. Nonetheless, in the GGAU relaxation, the Ti^{3+} states are separated from the CBM, so we can observe the different nature of the surface Ti and Ti^{3+} states. The fluorine states, for the surface and bulk systems, are located at the VB bottom (see Figure S4).

Fluorine inhibits the full charge transfer from the Ti atoms, leading one Ti^{3+} atom. These states are depicted on

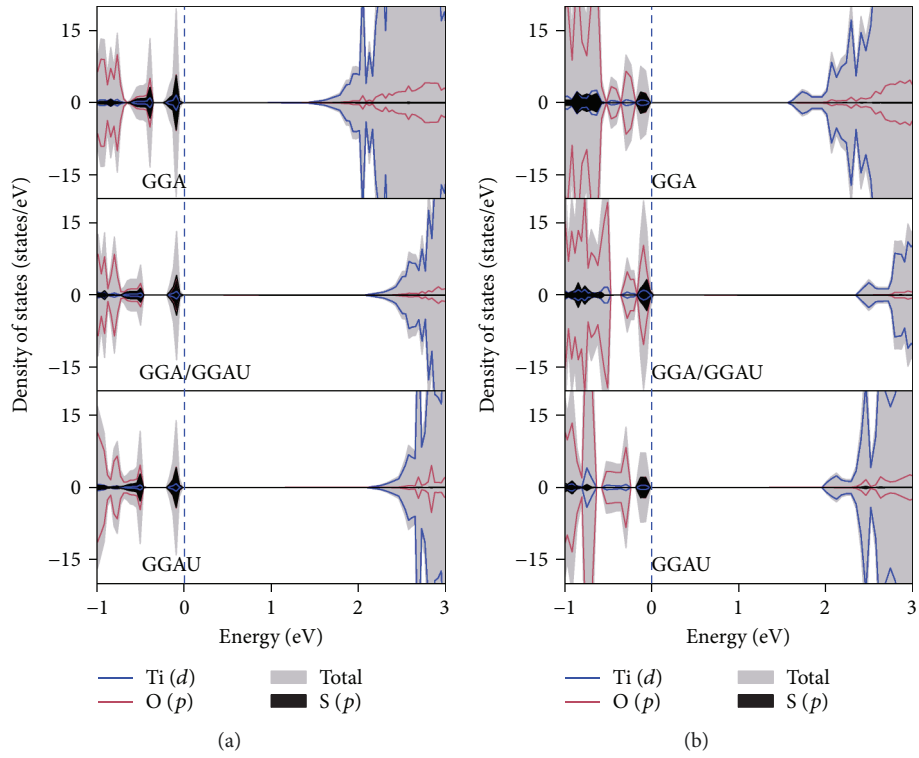

Figure 5: The total and partial density of states of the three relaxation methodologies for S-doped anatase TiO_2. (a) The bulk supercell. (b) The TiO_2 (101) surface.

Table 1: Summary of bandgaps (E_g) for the bulk and surface models for all doped and pristine TiO_2. Energy units are in eV.

Dopant	Bulk			Surface		
	GGA	GGA/GGAU	GGAU	GGA	GGA/GGAU	GGAU
C	2.44	2.66	2.66	1.87	2.36	2.30
N	2.00	2.80	2.77	1.85	2.29	2.30
F	2.19	2.89	2.89	1.63	2.00	2.30
S	1.80	2.51	2.55	1.69	2.40	2.08
Pure	2.19	2.81	2.76	1.85	2.31	2.25

the DOS for the small dopant concentration using the GGAU scheme, which localizes an occupied state without F 2*p* orbital participation; this means the electron is in the Ti 3*d* orbital.

The F-doping TiO_2 system must be treated with caution because the F-doping creates Ti^{3+} states, that is not adequately described by GGA functionals, as in the case of the oxygen vacancies [71], but hybrid functionals recover the physical picture [16]. Here, it has been shown that the PBE functional gives delocalized solutions with the bulk and surface models, which is consistent with reports where F distributes its unpaired electron towards neighbors Ti atoms [16, 35]. The GGAU scheme recovers the localization of Ti^{3+} with a lower computational cost compared with hybrid functionals.

3.4. S-Doped TiO_2. We have argued that the number of localized states—empty and occupied—and its electron distribution is directly related to the electron configuration of the dopant *p* orbitals; thus, we finally examined an element which is in the same oxygen group, the sulfur.

Table 2: Formation energy for anatase TiO_2 doped with the main group elements. Results obtained with the GGAU scheme.

Dopant	Formation energy (eV)	
	Bulk	Surface
C	3.52	3.30
N	3.36	1.98
F	1.85	2.45
S	5.81	3.01

Sulfur has 16 electrons and presents a similar electron distribution and oxidation state like oxygen, which leads to an energy bandgap with no empty states as Figure 5 shows

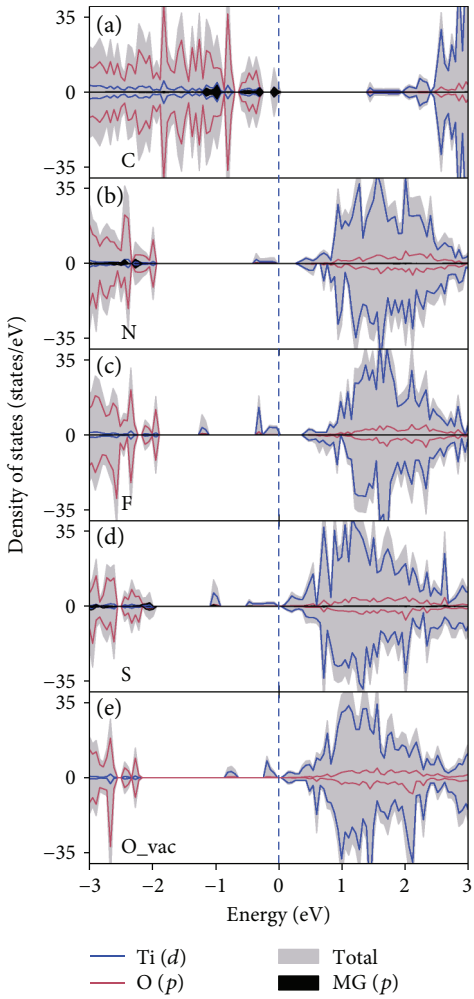

FIGURE 6: The total and partial density of states for pure and C-, N-, S-, F-doped anatase TiO_2 (101) with one oxygen vacancy. Results obtained with the GGAU methodology.

for all cases. The E_g reduction (see Table 1) is due to the occupied states that sulfur introduces at the top of the VB; it is important to note that spin-up and spin-down DOS are symmetrical (Figure S5) meaning all orbitals are fully occupied, confirming our configuration model. For the bulk system, these states are localized near the VB edge; this means there is some sulfur occupied states that show some repulsion from the occupied O 2*p* orbitals. This behavior is reflected in the high formation energy for S-doping (5.81 eV), as showed in Table 2. On the surface, in all cases, these states are closer to the VB than in the bulk. For the GGA/GGAU scheme, O *2p*, S *3p*, and Ti *3d* occupied states are mixed just below the Fermi level. In the GGAU case, the occupied states under Fermi level present S *3p* and Ti *3d* character only.

The covalent radius of S (1.02 Å) differs considerably from the O atom (0.73 Å), and then the orbital O 2*p* and S 3*p* hybridization is inhibited as GGAU scheme shows. The S-doping generates some occupied localized states, mainly S 3*p* character, below the Fermi level. However, although these states are occupied, they do not overlap with the VB (see Figure 5(a)). This may explain why experimentally high concentrations of sulfur are needed to enhance the photoactivity in the pollutant degradation [34]. If the sulfur substitution is located far from the surface, the charge carriers do not reach the surface, inhibiting the degradation activity. At high concentration, the probability that dopants reach the surface increases as well as the reactivity. This fact is carried out with large formation energies (5.81 eV, bulk) due to significant structural changes by S covalent radius.

The GGA/GGAU and GGAU methods give, for almost all cases, a good picture for the localized electronic states within the bandgap. However, the GGA/GGAU methodology has to be carefully treated because of the lack of ionic relaxation some states may not be well localized. It has been reported that the Hubbard *U* parameter depends heavily on the used geometry, so we encourage doing the full optimization GGAU methodology.

The Hubbard correction slightly widens the bandgap for all systems (see Table 1). *U* correlation is mandatory to describe TiO_2 systems if there is a hybridization between the dopant and Ti 3*d* orbitals. The Hubbard model is also necessary when unpaired electrons occupy Ti 3*d* states because the extra electron repulsion in the valence electrons localizes states below the CBM.

3.5. Oxygen Vacancies on Doped TiO_2 (101). We also studied the effect on the electronic structure of oxygen vacancies on the doped TiO_2 (101) surface systems. The formation energy of one oxygen vacancy follows the order: F (5.740) > S (5.734) > C (4.084) > N (3.963 eV). Experimentally, the oxygen vacancies are promoted when the surface is doped with N and C, which is consistent with our theoretical results [72–74].

Removing one oxygen atom from the pure TiO_2 surface yields Ti^{3+} states that are below the conduction band [71, 75] (see Figure 6(e)). C-doping shows a different behavior, that is, the two electrons available after removing the neutral oxygen go to the C 2*p* orbital (empty states generated by C-doping), above the valence band (see Figure 6(a)). Since oxygen and sulfur are isoelectronic, the oxygen vacancy on the S-doped system generates Ti^{3+} states just as with the pristine TiO_2 (101) (see Figure 6(d)).

For F-doping, there are three intrabandgap states, and one of them corresponds to the extra electron of fluorine compared to oxygen, which is in agreement with Czoska et al. [16] results. The other two states correspond to the ones generated by the oxygen vacancy. The electrons from the oxygen vacancies create Ti^{3+} species near the Fermi level; the Ti^{3+} state created by the F electron is the nearest to the valence band.

For N-doping, one electron from the oxygen vacancy locates at N 2*p* orbital; the other creates a Ti^{3+} state near the CB (see Figure 6(b)). C, as N atoms, accepts the extra charge derived from the oxygen vacancy. Zhang et al. [40] also found that the visible light photoactive centers of N-doped TiO_2 are the substitutional N species with a diamagnetic [O-Ti^{4+}-N^{3-}-Ti^{4+}-V_O^{-}] cluster containing an oxygen vacancy and an N atom. It has been shown that the charge excess can be trapped by N impurities leading to a

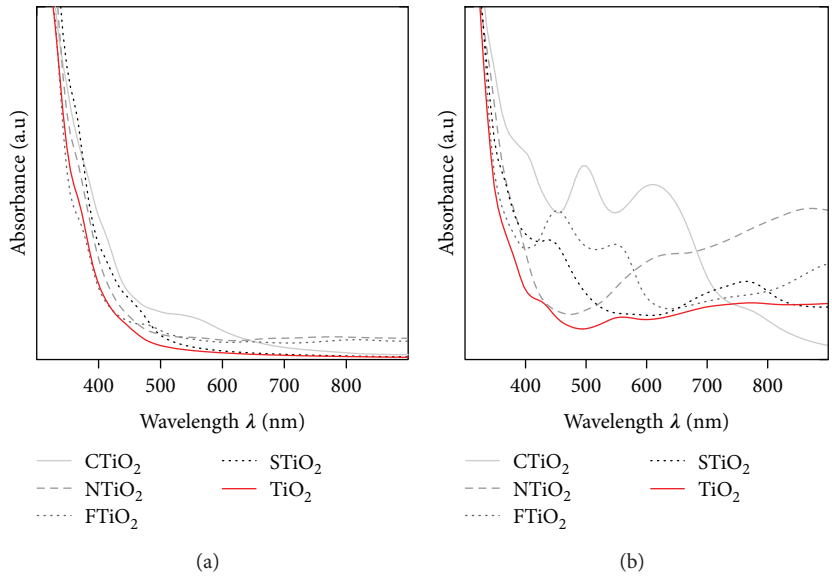

Figure 7: The UV-visible spectrum of anatase surface. (a) C-, N-, F-, and S-doped TiO_2 (101). (b) Doped surface with one oxygen vacancy. Results obtained with the GGAU methodology.

catalytic efficiency enhancement [74]. Finazzi et al. [66] reported a similar behavior when substituting two O atoms by N; the unpaired electrons fill the dopant N 2*p* states giving a closed shell configuration. The synergy between the dopants and oxygen vacancies cleans the gap, but for nitrogen aside to clean the gap, these new states are well mixed with the O 2*p* states from the valence band, so it enhanced the charge mobility.

For the C-doped TiO_2 bulk system, Kamisaka et al. [76] concluded that oxygen vacancies diminish the photocatalytic activity by filling the holes generated by the dopant, inhibiting the charge mobility. In our case, for the surface TiO_2 (101) anatase, C 2*p* states lie above the valence band, which is beneficial for the photocatalytic activity. Because the C dopant is localized near the surface, the generated charge carriers will already be at a reactive site, that is, these localized states may enhance the charge carrier lifetime.

3.6. Optical Response of Doped TiO_2 (101) with One Oxygen Vacancy. The optical absorption of the C-, N-, F-, and S-doped surface TiO_2 (101) was also determined (see Figure 7(a)). To correct the DFT gap underestimation, the optical absorption also includes the scissor operator (with a value of 0.44 eV). This method has been successfully applied to several materials [77–79]. The same scissor operator is used for the doped surface with and without oxygen vacancies.

The UV-visible spectrum (Figure 7(a)) agrees with the experimental data reported by Chen et al. [80], where the C-doping shows the maximum absorbance. In our case, there is a shoulder at $\lambda_{max} = 500$ nm (blue), which corresponds to transitions from valence band O 2*p* states to C 2*p* empty localized in the center of the bandgap (see Figures 3(b) and 6(a)). When the oxygen vacancy is considered, the optical activity in the visible region is significantly increased for doped TiO_2, which favors the generation of charge carriers using visible light (see Figure 7(b)).

Due to that oxygen vacancies are present in almost all synthesized TiO_2 materials, the simultaneous presence of main group elements and one oxygen vacancy is frequent. According to experimental results [80], when the nitrogen concentration increases, it also rises the oxygen vacancies and Ti^{3+}, leading to the enhancement of photocatalytic activity. From our theoretical results, N-doping presents the lowest formation energy of oxygen vacancies (3.963 eV). For the N-doped system with an oxygen vacancy, there are two shoulders at λ_{max} ~550 and 750 nm, which correspond to transitions from Ti 3*d* occupied states to Ti 3*d* empty states (see Figure 6(b)).

The F atom hinders the formation of oxygen vacancy. These results contrast with Hattori et al. [81] results. They stated that F ion promotes the formation of oxygen vacancies. The partial DOS (Figure 6(c)) shows that the Fermi level is displaced about 0.2 eV from the conduction band when an oxygen vacancy is present, which does not reduce the TiO_2 chemical potential. The F-doping without oxygen vacancy presents a similar optical activity than TiO_2 with oxygen vacancies, which agrees with experimental evidence that F-TiO_2 can hardly displace the light absorption towards the visible region. In spite of this, it has been reported that F-doped TiO_2 has catalytic activity under visible light. It is speculated that this activity may be due to other species like F_2 or HF adsorbed on the surface [36, 82].

For all the studied cases, oxygen vacancies on the TiO_2 (101) surface displace the light spectrum towards the visible region. A severe increase in the optical absorption intensity is obtained following the order C > N > F > S. The reason that F and S do not present a high photocatalytic efficiency is that they promote Ti^{3+} states; the charge carriers have not the oxidation potential required to form the $OH^{\bullet}$ species. The high

absorbance of C-doping in the visible light (Figure 7(b)) as well as the localized state above the bandgap explains why it is five times more efficient than N-doping in the degradation of 4-chlorophenol when it is used as an artificial light ($\lambda \geq 455$ nm) [33].

4. Conclusions

The electronic structure of the bulk and surface (101) models of anatase TiO_2 doped with the main group elements C, N, F, and S, with and without oxygen vacancies, was studied using DFT and the Hubbard U approach.

The GGA approach alone underestimated the bandgap for all cases, with a systematic failure of the method. The best and simplest method for describing the doped TiO_2 electronic structure is the ionic relaxation of the TiO_2 models with the GGA + U scheme, which obtains localized solutions at the same computational cost of the GGA approach.

Two ways for reducing the TiO_2 bandgap were identified. The first mechanism is broadening the VB or CB. The presence of occupied states near the VBM reduces the bandgap, and then less energy is required to excite electrons from VB to CB. The S-doping TiO_2 (101) is an example of that mechanism. A similar process can occur, but in the CB when the TiO_2 (101) surface is formed, the exposed Ti atoms present undercoordination, giving rise to empty states very close the CBM.

The second mechanism for reducing the bandgap is to generate localized states in the gap. However, this process has the inconvenience that these states may act as recombination centers. For example, the C- and N-doping form localized empty states in the gap. For the C-doping, the surface TiO_2 (101) presents a "cleaner" gap than the bulk TiO_2, which is favorable to eliminate recombination centers. Finally, the F-doping represents a similar case to oxygen vacancies, where the fluorine atom promotes the Ti^{3+} species formation, which appears below the CBM.

The number of valence electrons of the dopant element determines the number of states and its position within the gap when the O atom is replaced.

Both doping and oxygen vacancies on TiO_2 (101) displace the light spectrum towards the visible region. A great increase in the optical absorption intensity is obtained with the following order C > N > F > S. Therefore, the high catalytic activity of C-doping using visible radiation is consistent with its high absorption intensity generated by oxygen vacancies on the surface.

Data Availability

The data used to support the findings of this study are available from the corresponding author upon request.

Conflicts of Interest

The authors declare that they have no conflicts of interest.

Acknowledgments

Oscar Olvera-Neria thanks the CONACYT-México for the financial support for the project CB-2011-01/166246. The authors are indebted to the UAM Iztapalapa for the computing time in the Yoltla supercomputer. Julio César González-Torres is grateful to the CONACYT for the studentship granted to pursue his doctoral studies.

Supplementary Materials

Figure S1: the total and partial density of states of the three relaxation methodologies for anatase TiO_2. (a) The bulk supercell. (b) The TiO_2 (101) surface. The Fermi level corresponds to the zero energy. Figure S2: the total and partial density of states of the three relaxation methodologies for C-doped anatase TiO_2. (a) The bulk supercell. (b) The TiO_2 (101) surface. Figure S3: the total and partial density of states of the three relaxation methodologies for N-doped anatase TiO_2. (a) The bulk supercell. (b) The TiO_2 (101) surface. Figure S4: the total and partial density of states of the three relaxation methodologies for F-doped anatase TiO_2. (a) The bulk supercell. (b) The TiO_2 (101). Figure S5: the total and partial density of states of the three relaxation methodologies for S-doped anatase TiO_2. (a) The bulk supercell. (b) The TiO_2 (101) surface. *(Supplementary Materials)*

References

[1] M. Fujihira, Y. Satoh, and T. Osa, "Heterogeneous photocatalytic oxidation of aromatic compounds on TiO_2," *Nature*, vol. 293, no. 5829, pp. 206–208, 1981.

[2] A. Fujishima and K. Honda, "Electrochemical photolysis of water at a semiconductor electrode," *Nature*, vol. 238, no. 5358, pp. 37-38, 1972.

[3] T. Inoue, A. Fujishima, S. Konishi, and K. Honda, "Photoelectrocatalytic reduction of carbon dioxide in aqueous suspensions of semiconductor powders," *Nature*, vol. 277, no. 5698, pp. 637-638, 1979.

[4] S. Hamzezadeh-Nakhjavani, O. Tavakoli, S. P. Akhlaghi, Z. Salehi, P. Esmailnejad-Ahranjani, and A. Arpanaei, "Efficient photocatalytic degradation of organic pollutants by magnetically recoverable nitrogen-doped TiO_2 nanocomposite photocatalysts under visible light irradiation," *Environmental Science and Pollution Research*, vol. 22, no. 23, pp. 18859–18873, 2015.

[5] M. Romero-Sáez, L. Y. Jaramillo, R. Saravanan et al., "Notable photocatalytic activity of TiO_2-polyethylene nanocomposites for visible light degradation of organic pollutants," *Express Polymer Letters*, vol. 11, no. 11, pp. 899–909, 2017.

[6] T. Sreethawong, S. Ngamsinlapasathian, and S. Yoshikawa, "Positive role of incorporating P-25 TiO_2 to mesoporous-assembled TiO_2 thin films for improving photocatalytic dye degradation efficiency," *Journal of Colloid and Interface Science*, vol. 430, pp. 184–192, 2014.

[7] R. Sidaraviciute, E. Krugly, L. Dabasinskaite, E. Valatka, and D. Martuzevicius, "Surface-deposited nanofibrous TiO_2 for photocatalytic degradation of organic pollutants," *Journal of Sol-Gel Science and Technology*, vol. 84, no. 2, pp. 306–315, 2017.

[8] P. Haowei, L. Jingbo, L. Shu-Shen, and X. Jian-Bai, "First-principles study of the electronic structures and magnetic properties of 3d transition metal-doped anatase TiO_2," *Journal of Physics: Condensed Matter*, vol. 20, no. 12, article 125207, 2008.

[9] K. Song, X. Han, and G. Shao, "Electronic properties of rutile TiO_2 doped with 4d transition metals: first-principles study," *Journal of Alloys and Compounds*, vol. 551, pp. 118–124, 2013.

[10] S. Yang and H. Lee, "Determining the catalytic activity of transition metal-doped TiO_2 nanoparticles using surface spectroscopic analysis," *Nanoscale Research Letters*, vol. 12, no. 1, p. 582, 2017.

[11] P. Ribao, M. J. Rivero, and I. Ortiz, "TiO_2 structures doped with noble metals and/or graphene oxide to improve the photocatalytic degradation of dichloroacetic acid," *Environmental Science and Pollution Research*, vol. 24, no. 14, pp. 12628–12637, 2017.

[12] S. N. R. Inturi, T. Boningari, M. Suidan, and P. G. Smirniotis, "Visible-light-induced photodegradation of gas phase acetonitrile using aerosol-made transition metal (V, Cr, Fe, Co, Mn, Mo, Ni, Cu, Y, Ce, and Zr) doped TiO_2," *Applied Catalysis B: Environmental*, vol. 144, pp. 333–342, 2014.

[13] D. Toprek, V. Koteski, J. Belošević-Čavor, V. Ivanovski, and A. Umićević, "Ab initio study of electronic and optical properties of *Fe* doped anatase *TiO_2* (101) surface," vol. 1120, pp. 17–23, 2017.

[14] Y. Lin, Z. Jiang, C. Zhu et al., "The electronic structure, optical absorption and photocatalytic water splitting of (Fe + Ni)-codoped TiO_2: a DFT+U study," *International Journal of Hydrogen Energy*, vol. 42, no. 8, pp. 4966–4976, 2017.

[15] J. Atanelov, C. Gruber, and P. Mohn, "The electronic and magnetic structure of *p*-element (C,N) doped rutile-TiO_2; a hybrid DFT study," *Computational Materials Science*, vol. 98, pp. 42–50, 2015.

[16] A. M. Czoska, S. Livraghi, M. Chiesa et al., "The nature of defects in fluorine-doped TiO_2," *Journal of Physical Chemistry C*, vol. 112, no. 24, pp. 8951–8956, 2008.

[17] H. Gao, J. Zhou, D. Dai, and Y. Qu, "Photocatalytic activity and electronic structure analysis of N-doped anatase TiO_2: a combined experimental and theoretical study," *Chemical Engineering & Technology*, vol. 32, no. 6, pp. 867–872, 2009.

[18] K. Yang, Y. Dai, and B. Huang, "Study of the nitrogen concentration influence on N-doped TiO_2 anatase from first-principles calculations," *The Journal of Physical Chemistry C*, vol. 111, no. 32, pp. 12086–12090, 2007.

[19] H. Hou, F. Gao, M. Shang et al., "Enhanced visible-light responsive photocatalytic activity of N-doped TiO_2 thoroughly mesoporous nanofibers," *Journal of Materials Science: Materials in Electronics*, vol. 28, no. 4, pp. 3796–3805, 2017.

[20] S. K. Kassahun, Z. Kiflie, D. W. Shin, S. S. Park, W. Y. Jung, and Y. R. Chung, "Facile low temperature immobilization of N-doped TiO_2 prepared by sol–gel method," *Journal of Sol-Gel Science and Technology*, vol. 83, no. 3, pp. 698–707, 2017.

[21] J. Zhao, W. Li, X. Li, and X. Zhang, "Low temperature synthesis of water dispersible F-doped TiO_2 nanorods with enhanced photocatalytic activity," *RSC Advances*, vol. 7, no. 35, pp. 21547–21555, 2017.

[22] X. Zhang, Z. Li, Z. Zhan, and L. Di, "Preparation of F-doped TiO_2 photocatalysts by gas–liquid plasma at atmospheric pressure," *Topics in Catalysis*, vol. 60, no. 12-14, pp. 980–986, 2017.

[23] R. Ata, O. Sacco, V. Vaiano, L. Rizzo, G. Y. Tore, and D. Sannino, "Visible light active N-doped TiO_2 immobilized on polystyrene as efficient system for wastewater treatment," *Journal of Photochemistry and Photobiology A: Chemistry*, vol. 348, pp. 255–262, 2017.

[24] Y. H. Lin, H. T. Hsueh, C. W. Chang, and H. Chu, "The visible light-driven photodegradation of dimethyl sulfide on S-doped TiO_2: characterization, kinetics, and reaction pathways," *Applied Catalysis B: Environmental*, vol. 199, pp. 1–10, 2016.

[25] D. Guerrero-Araque, D. Ramírez-Ortega, P. Acevedo-Peña, F. Tzompantzi, H. A. Calderón, and R. Gómez, "Interfacial charge-transfer process across ZrO_2-TiO_2 heterojunction and its impact on photocatalytic activity," *Journal of Photochemistry and Photobiology A: Chemistry*, vol. 335, pp. 276–286, 2017.

[26] I. Permadani, D. A. Phasa, A. W. Pratiwi, and F. Rahmawati, "The composite of ZrO_2-TiO_2 produced from local zircon sand used as a photocatalyst for the degradation of methylene blue in a single batik dye wastewater," *Bulletin of Chemical Reaction Engineering & Catalysis*, vol. 11, no. 2, pp. 133–139, 2016.

[27] K. Nakata and A. Fujishima, "TiO_2 photocatalysis: design and applications," *Journal of Photochemistry and Photobiology C: Photochemistry Reviews*, vol. 13, no. 3, pp. 169–189, 2012.

[28] K. Hashimoto, H. Irie, and A. Fujishima, "TiO_2 photocatalysis: a historical overview and future prospects," *Japanese Journal of Applied Physics*, vol. 44, no. 12, article 8269, 2005.

[29] M. A. Henderson, "A surface science perspective on TiO_2 photocatalysis," *Surface Science Reports*, vol. 66, no. 6-7, pp. 185–297, 2011.

[30] W. Shockley and W. T. Read, "Statistics of the recombinations of holes and electrons," *Physical Review*, vol. 87, no. 5, pp. 835–842, 1952.

[31] R. N. Hall, "Electron-hole recombination in germanium," *Physical Review*, vol. 87, no. 2, pp. 387–387, 1952.

[32] R. Asahi, T. Morikawa, T. Ohwaki, K. Aoki, and Y. Taga, "Visible-light photocatalysis in nitrogen-doped titanium oxides," *Science*, vol. 293, no. 5528, pp. 269–271, 2001.

[33] S. Sakthivel and H. Kisch, "Daylight photocatalysis by carbon-modified titanium dioxide," *Angewandte Chemie International Edition*, vol. 42, no. 40, pp. 4908–4911, 2003.

[34] F. H. Tian and C. B. Liu, "DFT description on electronic structure and optical absorption properties of anionic S-doped anatase TiO_2," *The Journal of Physical Chemistry B*, vol. 110, no. 36, pp. 17866–17871, 2006.

[35] T. Yamaki, T. Umebayashi, T. Sumita et al., "Fluorine-doping in titanium dioxide by ion implantation technique," *Nuclear Instruments and Methods in Physics Research Section B: Beam Interactions with Materials and Atoms*, vol. 206, pp. 254–258, 2003.

[36] J. C. Yu, J. Yu, W. Ho, Z. Jiang, and L. Zhang, "Effects of F^- doping on the photocatalytic activity and microstructures of nanocrystalline TiO_2 powders," *Chemistry of Materials*, vol. 14, no. 9, pp. 3808–3816, 2002.

[37] U. Diebold, "The surface science of titanium dioxide," *Surface Science Reports*, vol. 48, no. 5-8, pp. 53–229, 2003.

[38] K. Iijima, M. Goto, S. Enomoto et al., "Influence of oxygen vacancies on optical properties of anatase TiO_2 thin films," *Journal of Luminescence*, vol. 128, no. 5-6, pp. 911–913, 2008.

[39] R. Chandana, P. Mohanty, A. C. Pandey, and N. C. Mishra, "Oxygen vacancy induced structural phase transformation in

TiO_2 nanoparticles," *Journal of Physics D: Applied Physics*, vol. 42, no. 20, article 205101, 2009.

[40] Z. Zhang, X. Wang, J. Long, Q. Gu, Z. Ding, and X. Fu, "Nitrogen-doped titanium dioxide visible light photocatalyst: spectroscopic identification of photoactive centers," *Journal of Catalysis*, vol. 276, no. 2, pp. 201–214, 2010.

[41] L. Chen, Q. Gu, L. Hou et al., "Molecular p-n heterojunction-enhanced visible-light hydrogen evolution over a N-doped TiO_2 photocatalyst," *Catalysis Science & Technology*, vol. 7, no. 10, pp. 2039–2049, 2017.

[42] G. Kresse and J. Furthmüller, "Efficient iterative schemes for *ab initio* total-energy calculations using a plane-wave basis set," *Physical Review B*, vol. 54, no. 16, pp. 11169–11186, 1996.

[43] G. Kresse and J. Furthmüller, "Efficiency of ab-initio total energy calculations for metals and semiconductors using a plane-wave basis set," *Computational Materials Science*, vol. 6, no. 1, pp. 15–50, 1996.

[44] P. Hohenberg and W. Kohn, "Inhomogeneous electron gas," *Physical Review*, vol. 136, no. 3B, pp. B864–B871, 1964.

[45] W. Kohn and L. J. Sham, "Self-consistent equations including exchange and correlation effects," *Physical Review*, vol. 140, no. 4A, pp. A1133–A1138, 1965.

[46] J. P. Perdew, K. Burke, and M. Ernzerhof, "Generalized gradient approximation made simple," *Physical Review Letters*, vol. 77, no. 18, pp. 3865–3868, 1996.

[47] J. P. Perdew, K. Burke, and M. Ernzerhof, "Generalized gradient approximation made simple [Phys. Rev. Lett. 77, 3865 (1996)]," *Physical Review Letters*, vol. 78, no. 7, pp. 1396–1396, 1997.

[48] A. D. Becke, "Density-functional exchange-energy approximation with correct asymptotic behavior," *Physical Review A*, vol. 38, no. 6, pp. 3098–3100, 1988.

[49] A. D. Becke, "Density functional calculations of molecular bond energies," *Journal of Chemical Physics*, vol. 84, no. 8, pp. 4524–4529, 1986.

[50] J. P. Perdew, "Density-functional approximation for the correlation energy of the inhomogeneous electron gas," *Physical Review B*, vol. 33, no. 12, pp. 8822–8824, 1986.

[51] J. P. Perdew and W. Yue, "Accurate and simple density functional for the electronic exchange energy: generalized gradient approximation," *Physical Review B*, vol. 33, no. 12, pp. 8800–8802, 1986.

[52] J. P. Perdew, "Density functional theory and the band gap problem," *International Journal of Quantum Chemistry*, vol. 28, no. S19, pp. 497–523, 1985.

[53] S. L. Dudarev, G. A. Botton, S. Y. Savrasov, C. J. Humphreys, and A. P. Sutton, "Electron-energy-loss spectra and the structural stability of nickel oxide: an LSDA+U study," *Physical Review B*, vol. 57, no. 3, pp. 1505–1509, 1998.

[54] C. I. N. Morgade and G. F. Cabeza, "Synergetic interplay between metal (Pt) and nonmetal (C) species in codoped TiO_2: a DFT+U study," *Computational Materials Science*, vol. 111, pp. 513–524, 2016.

[55] C. J. Calzado, N. C. Hernández, and J. F. Sanz, "Effect of on-site Coulomb repulsion term U on the band-gap states of the reduced rutile (110) TiO_2 surface," *Physical Review B*, vol. 77, no. 4, article 045118, 2008.

[56] P. E. Blöchl, "Projector augmented-wave method," *Physical Review B*, vol. 50, no. 24, pp. 17953–17979, 1994.

[57] G. Kresse and D. Joubert, "From ultrasoft pseudopotentials to the projector augmented-wave method," *Physical Review B*, vol. 59, no. 3, pp. 1758–1775, 1999.

[58] M. Lazzeri, A. Vittadini, and A. Selloni, "Structure and energetics of stoichiometric TiO_2 anatase surfaces," *Physical Review B*, vol. 63, no. 15, article 155409, 2001.

[59] M. Lazzeri, A. Vittadini, and A. Selloni, "Erratum: Structure and energetics of stoichiometric TiO_2 anatase surfaces [Phys. Rev. B 63, 155409 (2001)]," *Physical Review B*, vol. 65, no. 11, article 119901, 2002.

[60] V. Wang, "VASPKIT, postprocessing tool for VASP code," 2014, http://vaspkit.sourceforge.net.

[61] M. Gajdoš, K. Hummer, G. Kresse, J. Furthmüller, and F. Bechstedt, "Linear optical properties in the projector-augmented wave methodology," *Physical Review B*, vol. 73, no. 4, article 045112, 2006.

[62] M. Horn, C. F. Schwerdtfeger, and E. P. Meagher, "Refinement of the structure of anatase at several temperatures*," *Zeitschrift für Kristallographie*, vol. 136, no. 3-4, pp. 273–281, 1972.

[63] K. Yang, Y. Dai, B. Huang, and M.-H. Whangbo, "On the possibility of ferromagnetism in carbon-doped anatase TiO_2," *Applied Physics Letters*, vol. 93, no. 13, p. 132507, 2008.

[64] X. J. Ye, W. Zhong, M. H. Xu, X. S. Qi, C. T. Au, and Y. W. Du, "The magnetic property of carbon-doped TiO_2," *Physics Letters A*, vol. 373, no. 40, pp. 3684–3687, 2009.

[65] Z. Lin, A. Orlov, R. M. Lambert, and M. C. Payne, "New insights into the origin of visible light photocatalytic activity of nitrogen-doped and oxygen-deficient anatase TiO_2," *The Journal of Physical Chemistry B*, vol. 109, no. 44, pp. 20948–20952, 2005.

[66] E. Finazzi, C. Di Valentin, A. Selloni, and G. Pacchioni, "First principles study of nitrogen doping at the anatase TiO_2(101) surface," *The Journal of Physical Chemistry C*, vol. 111, no. 26, pp. 9275–9282, 2007.

[67] N. C. Khang, N. Van Khanh, N. H. Anh, D. T. Nga, and N. Van Minh, "The origin of visible light photocatalytic activity of N-doped and weak ferromagnetism of Fe-doped TiO_2 anatase," *Advances in Natural Sciences: Nanoscience and Nanotechnology*, vol. 2, no. 1, article 015008, 2011.

[68] L. Chun-Ming, X. Xia, Z. Yan, J. Yong, and Z. Xiao-Tao, "Magnetism of a nitrogen-implanted TiO_2 single crystal," *Chinese Physics Letters*, vol. 28, no. 12, article 127201, 2011.

[69] D. Dvoranová, V. Brezová, M. Mazúr, and M. A. Malati, "Investigations of metal-doped titanium dioxide photocatalysts," *Applied Catalysis B: Environmental*, vol. 37, no. 2, pp. 91–105, 2002.

[70] C. Di Valentin, E. Finazzi, G. Pacchioni et al., "Density functional theory and electron paramagnetic resonance study on the effect of N–F codoping of TiO_2," *Chemistry of Materials*, vol. 20, no. 11, pp. 3706–3714, 2008.

[71] N. S. Portillo-Vélez, O. Olvera-Neria, I. Hernández-Pérez, and A. Rubio-Ponce, "Localized electronic states induced by oxygen vacancies on anatase TiO2 (101) surface," *Surface Science*, vol. 616, pp. 115–119, 2013.

[72] M. Batzill, E. H. Morales, and U. Diebold, "Influence of nitrogen doping on the defect formation and surface properties of TiO_2 rutile and anatase," *Physical Review Letters*, vol. 96, no. 2, article 026103, 2006.

[73] C. Di Valentin, G. Pacchioni, and A. Selloni, "Theory of carbon doping of titanium dioxide," *Chemistry of Materials*, vol. 17, no. 26, pp. 6656–6665, 2005.

[74] C. Di Valentin, G. Pacchioni, A. Selloni, S. Livraghi, and E. Giamello, "Characterization of paramagnetic species in N-doped TiO_2 powders by EPR spectroscopy and DFT calculations," *The Journal of Physical Chemistry B*, vol. 109, no. 23, pp. 11414–11419, 2005.

[75] G. Pacchioni, "Oxygen vacancy: the invisible agent on oxide surfaces," *Chemphyschem*, vol. 4, no. 10, pp. 1041–1047, 2003.

[76] H. Kamisaka, T. Adachi, and K. Yamashita, "Theoretical study of the structure and optical properties of carbon-doped rutile and anatase titanium oxides," *The Journal of Chemical Physics*, vol. 123, no. 8, article 084704, 2005.

[77] M. Guo and J. Du, "First-principles study of electronic structures and optical properties of Cu, Ag, and Au-doped anatase TiO_2," *Physica B: Condensed Matter*, vol. 407, no. 6, pp. 1003–1007, 2012.

[78] J. Li, S.-H. Wei, S.-S. Li, and J.-B. Xia, "Design of shallow acceptors in ZO: first-principles band-structure calculations," *Physical Review B*, vol. 74, no. 8, article 081201, 2006.

[79] H. Weng, J. Dong, T. Fukumura, M. Kawasaki, and Y. Kawazoe, "First principles investigation of the magnetic circular dichroism spectra of co-doped anatase and rutile TiO_2," *Physical Review B*, vol. 73, no. 12, article 121201, 2006.

[80] D. Chen, Z. Jiang, J. Geng, Q. Wang, and D. Yang, "Carbon and nitrogen co-doped TiO_2 with enhanced visible-light photocatalytic activity," *Industrial & Engineering Chemistry Research*, vol. 46, no. 9, pp. 2741–2746, 2007.

[81] A. Hattori, K. Shimoda, H. Tada, and S. Ito, "Photoreactivity of sol–gel TiO_2 films formed on soda-lime glass substrates: effect of SiO_2 underlayer containing fluorine," *Langmuir*, vol. 15, no. 16, pp. 5422–5425, 1999.

[82] H. Sun, S. Wang, H. M. Ang, M. O. Tadé, and Q. Li, "Halogen element modified titanium dioxide for visible light photocatalysis," *Chemical Engineering Journal*, vol. 162, no. 2, pp. 437–447, 2010.